PNAS RESEARCH ARTICLE | APPLIED BIOLOGICAL SCIENCES

Extending the G1 phase improves the production of lipophilic compounds in yeast by boosting enzyme expression and increasing cell size

He Hao[a,b,1], Mingdong Yao[a,b,1], Ying Wang[a,b], Chenglong Zhang[a,b], Zihe Liu[c], Jens Nielsen[c,d,e,2], Shuobo Shi[c,2], Wenhai Xiao[a,b,f,g,2], and Yingjin Yuan[a,b]

Affiliations are included on p. 8.

Contributed by Jens Nielsen; received July 5, 2024; accepted October 12, 2024; reviewed by Hal S. Alper and Jack T. Pronk

Cell phase engineering can significantly impact protein synthesis and cell size, potentially enhancing the production of lipophilic products. This study investigated the impact of G1 phase extension on resource allocation, metabolic functions, and the unfolded protein response (UPR) in yeast, along with the potential for enhancing the production of lipophilic compounds. In brief, the regulation of the G1 phase was achieved by deleting *CLN3* (G1 cyclin) in various yeast strains. This modification resulted in a 83% increase in cell volume, a 76.9% increase in dry cell weight, a 82% increase in total protein content, a 41% increase in carotenoid production, and a 159% increase in fatty alcohol production. Transcriptomic analysis revealed significant upregulation of multiple metabolic pathways involved in acetyl-CoA (acetyl coenzyme A) synthesis, ensuring an ample supply of precursors for the synthesis of lipophilic products. Furthermore, we observed improved protein synthesis, attributed to UPR activation during the prolonged G1 phase. These findings not only enhanced our understanding and application of yeast's capacity to synthesize lipophilic compounds in applied biotechnology but also offered unique insights into cellular behavior during the modified G1 phase, particularly regarding the UPR response, for basic research. This study demonstrates the potential of G1 phase intervention to increase the yield of hydrophobic compounds in yeast, providing a promising direction for further research.

G1 phase | metabolic engineering | synthetic biology | lipophilic products | cell size

Significance

Cells go through four phases in the cell cycle. During the G1 phase, the cell grows in size, synthesizes proteins, and prepares for cell division. However, the impact of G1 phase interventions remains underexplored, leaving a gap in our understanding of how cell cycle dynamics influence cell metabolism. Here, we report that prolonging the G1 phase in yeast increases cell size and enhances lipid and protein content, significantly facilitating the production of lipophilic products. These compounds constitute a large group of molecules that can be utilized for health and energy applications. By uncovering the underlying mechanisms, our work enhances the understanding of cell behavior and provides valuable insights into adjusting cell cycle for industrial use of yeast.

The G1 phase of *Saccharomyces cerevisiae* plays a pivotal role in cell growth and the preparatory processes for cell division. During this stage, a series of regulatory processes are initiated that control cell size, metabolic activity, protein synthesis, and overall physiology (1). However, the underlying reasons for these cellular responses and their potential applications in biomanufacturing have not been fully investigated.

Previous studies have highlighted the significance of the G1 phase in regulating various physiological processes, particularly in coordinating cell size and metabolism (2). The G1 phase plays a central role in controlling cell size; smaller cells undergo a longer G1 phase to reach the appropriate size before passing the cell size checkpoint (3). This intricate process is orchestrated by cyclin-dependent kinases (CDKs) and their inhibitors and activators, all of which play pivotal roles in normal cell cycle progression and significantly affect cell size (4). The G1 cyclin Cln3 plays a central role in regulating the G1 phase duration of cells by forming the Cln3–Cdk1 complex (5), leading to the release of the transcription factor SBF. This release facilitates the cell's transition into the subsequent S phase. In *S. cerevisiae*, the Cln3 level remains relatively constant as the cell size changes (6), whereas the level of the Cln3 inhibitor Whi5 decreases as the cells grow in the G1 phase (7). This phenomenon creates a cell size threshold at which Whi5 no longer inhibits Cln3 activity (7) (Fig. 1*A*). When the cell cycle is interrupted by chemical or genetic interference, the size of the cell continues to increase. In yeast, there is a parallel increase in cell volume and RNA and protein biosynthesis within a specific range (8). This synchronization implies that larger cells have a distinct advantage as cell factories, due to elevated levels of protein expression as well as expanded storage compartments for intracellular products, including lipophilic compounds. For example, in a previous study, activation of the unfolded protein response (UPR) was shown to facilitate protein synthesis, thereby enhancing the production of the lipophilic compound parthenolide (9). Additionally, expanding the storage space for lipophilic compounds supported a higher production of lipophilic terpenoids (10, 11).

Due to the enhanced protein synthesis ability during the prolonged G1 phase, key enzymes involved in product biosynthesis pathways are more likely to be expressed at

Author contributions: S.S., W.X., and Y.Y. designed research; H.H., M.Y., and Y.W. performed research; H.H., M.Y., Y.W., C.Z., Z.L., J.N., S.S., and W.X. analyzed data; J.N. edited paper; Y.Y. financed; and H.H., M.Y., S.S., W.X., and Y.Y. wrote the paper.

Reviewers: H.S.A., University of Texas at Austin; and J.T.P., Technische Universiteit Delft.

The authors declare no competing interest.

[1]H.H. and M.Y. contributed equally to this work.

[2]To whom correspondence may be addressed. Email: jni@bii.dk, shishuobo@mail.buct.edu.cn, or wenhai.xiao@tju.edu.cn.

This article contains supporting information online at https://www.pnas.org/lookup/suppl/doi:10.1073/pnas.2413486121/-/DCSupplemental.

Published November 13, 2024.

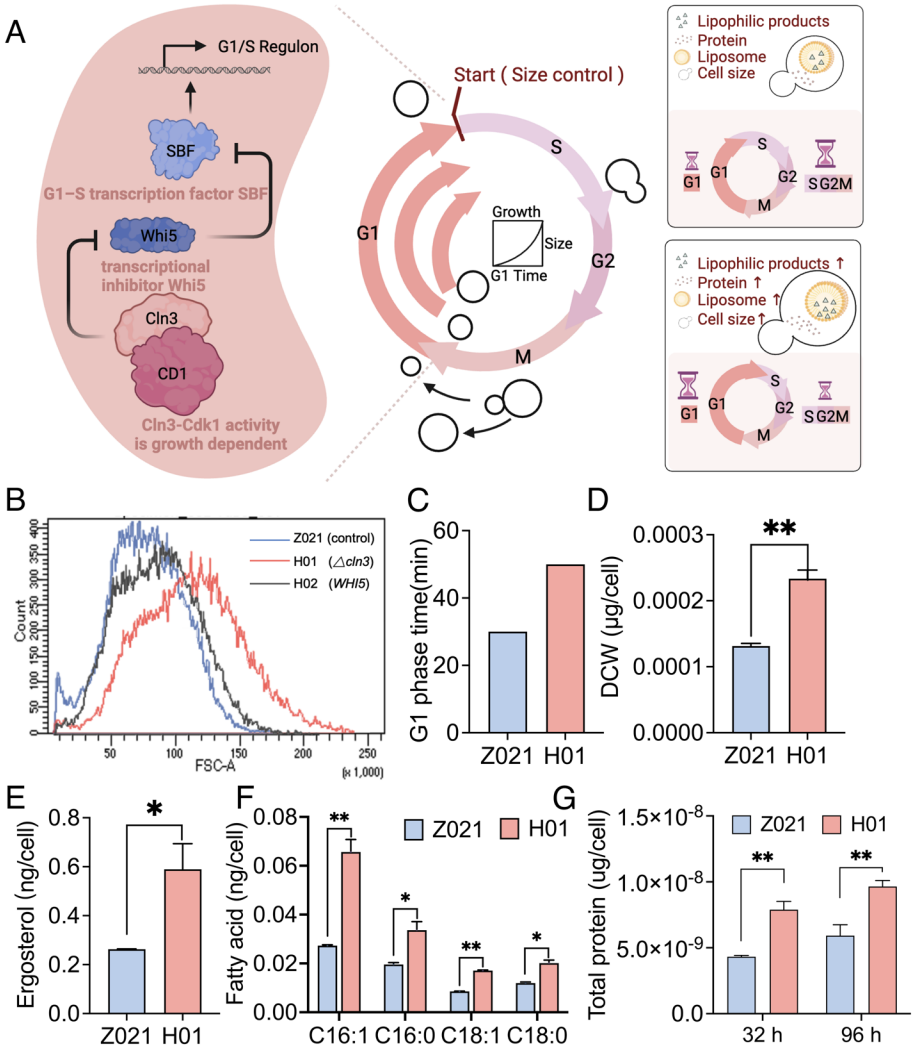

Fig. 1. Prolonging the G1 phase to increase cell size and protein synthesis. (*A*) Overview of cell cycle progression and the G1/S transition in yeast. Extension of the G1 phase results in increased cell size, as well as enhanced production of proteins, liposomes, and lipophilic products. (*B*) An analysis of the influence of cyclin genes (*WHI5* and *CLN3*) on cell size in yeast. Z021, the control strain, harbors a carotenoid pathway controlled by the *GAL* promoter; H01, Z021 with the *CLN3* gene knocked out; H02, Z021 overexpressing the *WHI5* gene. FSC–A: Forward Scatter–Area. (*C*) Comparison of G1 phase durations between Z021 and H01. (*D*) Comparison of dry cell weight (DCW) between Z021 and H01. (*E* and *F*) Examinations of ergosterol (*E*) and fatty acid (*F*) levels in Z021 and H01. C16:1, Palmitoleic acid; C16:0, Palmitic acid; C18:1, Oleic acid; C18:0, Stearic acid. (*G*) Comparison of total protein content between Z021 and H01. The total protein content is defined as the sum of all proteins obtained after the cell has been disrupted. The data in *B*–*F* were obtained by sampling and quantification of cells cultured in YPD medium at 96 h. The data in *G* were obtained by sampling and quantification of cells cultured in YPD medium at 32 h and 96 h. *SI Appendix*, Table S1 presents the data from *E*–*G* in both the unit of per biomass and per cell. The data are representative of three independent experiments performed in triplicate. Statistical analysis was performed using a two-tailed Student's *t* test (*$P < 0.05$, **$P < 0.01$, ***$P < 0.001$). The error bars represent the SD from the mean.

higher levels. However, endoplasmic reticulum (ER) stress arises when the ER's protein folding capacity cannot meet the cell's protein synthesis demands, triggering a series of responses, such as UPR and increased lipid synthesis (12). Additionally, in cells with a prolonged G1 phase, metabolic flux must be redistributed to accommodate the biosynthesis of cellular components necessary for maintaining a larger cell size. It remains unclear how cells respond to a prolonged G1 phase, as a complex communication network connects nutrient signaling pathways with cell cycle control networks (13–15). Historically, research on the cell cycle has focused primarily on basic cell physiology, but it also shows promising potential in biomanufacturing in recent time. For instance, Bezold et al. (16) reported that photogenetic intervention in the G2 phase of the budding yeast cell cycle significantly increased the production of valuable chemicals, though the underlying mechanism remains unresolved. Notably, interventions in the G1 phase have yet to be studied in applied biotechnology, leaving the relationship between cell cycle dynamics and cell factory performance largely unexplored.

Now lipophilic compounds have a wide range of applications, with fatty acid derivatives and terpenoids being two of the most important groups. These compounds consistently attract interest in the development of cell factories for applied biotechnology. In this study, we selected carotenoids and fatty alcohols as two representative lipophilic products. Our study illuminates the intricate relationships between the yeast cell cycle, cell size, metabolic changes, protein synthesis, and lipophilic compound production. By elucidating the underlying mechanisms and identifying potential regulatory targets, our findings not only broaden our understanding of cell behavior but also provide valuable insights for optimizing biological production processes and increasing the production of lipophilic compounds in yeast.

Results

Prolonging the G1 Phase to Increase Cell Size and Protein Synthesis. Given the critical role of the G1 cyclin Cln3 and its inhibitor Whi5 in controlling the G1 phase (4–7) (Fig. 1*A*), the

WHI5 and *CLN3* genes were selected as targets for extending the G1 phase and modulating cell size. Since carotenoid accumulation is influenced by cell size, a carotenoid-producing strain, Z021, was initially constructed to evaluate the effects of regulating the G1 phase. In this strain, all genes of the carotenoid pathway are controlled by the *GAL* promoter, and in the absence of galactose, the carotenoid pathway is inactive. Details of strain construction are provided in *SI Appendix*.

Two strategies were implemented: knockout of *CLN3* in the Z021 strain (resulting in the H01 strain) and overexpression of *WHI5* in the Z021 strain (resulting in the $H0_2$ strain). Flow cytometry analysis confirmed that *CLN3* knockout significantly increased cell size, while *WHI5* overexpression did not clearly affect cell size (Fig. 1*B*). Subsequent testing revealed a G1 phase extension of more than 20 min following *CLN3* knockout, as illustrated in Fig. 1*C* and *SI Appendix*, Fig. S1. This extension correlated with a visible increase in the volume of H01 cells under a 100× magnification, (*SI Appendix*, Fig. S2*A*). Moreover, the cell diameter increased from 3.42 μm to 4.18 μm, representing a substantial increase of 22% (*SI Appendix*, Fig. S2*B*). Remarkably, even a modest increase in cell diameter translated to a substantial increase in cell volume, providing ample storage space for target products. Here, an increase of 22% in cell diameter corresponded to an approximate 83% increase in cell volume, assuming yeast cells are spherical. Furthermore, the dry weight of the individual cells increased from 0.00013 ng/cell to 0.00023 ng/cell, representing a notable increase of 76.9% (Fig. 1*D*). Based on these observations, we hypothesize that the change in cell size was not due to environmental water uptake but rather to an increase in cellular constituents. Specifically, H01 also exhibited higher levels of fatty acids and sterols, which are key components of cell membranes (stationary phase cell samples were obtained and analyzed, Fig. 1 *E* and *F*). The unsaturation index of the cell (the ratio of unsaturated fatty acids to total fatty acids in the cell) increased from 0.53 to 0.61. Since unsaturated fatty acids determine membrane fluidity, we propose that the increase in membrane fluidity is induced when the cell becomes larger. The potential benefits of higher membrane fluidity include facilitating the function of membrane-bound enzymes, which can catalyze the conversion of lipophilic substrates, and reducing the cytotoxic effects of lipophilic products (17).

Notably, the production of proteins is intricately intertwined with both the cell division rate and cell size (18). A previous study reported that cell volume and protein biosynthesis increase in parallel within a specific range (4). As expected, the total protein content of H01 was significantly higher than that of Z021. In the exponential growth phase, H01 exhibited an impressive 82% increase in total protein content compared with Z021; in the stationary phase, the total protein content of H01 was 63% greater than that of Z021 (Fig. 1*G*). The enhanced capacity for protein synthesis may facilitate the expression of exogenous enzymes, while the increased cell volume could offer additional storage space for products. It is important to note that in Z021 and H01, the mass of an average cell, along with the protein content within that cell, essentially scales with cell size. This suggests that the protein content per gram of biomass for the two strains is not substantially different (*SI Appendix*, Table S1).

Having assessed the effect of cell size regulation in H01, we next evaluated the potential of *CLN3* deletion as a universal tool for modulating cell size. Using the same strategy, we engineered eight additional *S. cerevisiae* variants of different sizes from global isolates in nature (19). As depicted in *SI Appendix*, Fig. S3, these strains achieved varying degrees of cell expansion, ranging from 18 to 55% in diameter, supporting the idea that yeast cell size could be regulated by *CLN3* deletion.

Nutrient-Dependent Trade-Offs in Protein Production, Cell Division, and Reproduction Rates. Understanding the intricate relationships among protein production, cell division rate, and cell size can be used as a promising guidance for optimizing the efficiency of cell factories (20), as these factors are fundamentally linked to cell biomass (21). Perturbations in the cell cycle can potentially disrupt the balance between cell growth and reproduction, necessitating a comprehensive understanding of how these processes impact growth and reproductive dynamics.

On solid yeast extract peptone dextrose (YPD) medium, both the Z021 and H01 strains exhibited nearly identical growth patterns (Fig. 2*A*). However, in liquid medium, there was a concomitant extension of the exponential growth phase (Fig. 2*B*). This phenomenon was further investigated by assessing the yeast budding index (Fig. 2*C*), which revealed a decrease in cell division and proliferation rates. Cell growth encompasses the overall increase in cellular mass, comprising all the intracellular protein molecules constituting the cell mass and those serving as catalysts. However, according to previous findings (18), cells undergoing rapid growth may not reach their maximum protein production capacity, suggesting that decreased growth could signify a shift toward enhanced protein synthesis (22). Hence, the extension of the exponential growth and decrease in the growth rate may offer an opportunity to enhance growth-coupled production. Moreover, the increase in the dry cell weight (DCW) of H01 (Fig. 2*B*) can be attributed to the hypothesis that while the decrease in cell division led to lower cell numbers (*SI Appendix*, Fig. S4), the increase in protein biosynthesis compensated for this change, thereby improving biomass levels.

Protein production is a major consumer of energy and nutrients (18). While the rate of glucose consumption remained unchanged in H01, a difference in ethanol metabolism was observed following the switch in carbon sources (Fig. 2*D*). Specifically, the H01 strain exhibited accelerated ethanol utilization compared to Z021. This observation in the difference of ethanol utilization was consistent with the upregulation of *ADH1* in subsequent transcriptome analysis (Fig. 3*B*). The difference in ethanol consumption was also evident when the cells were incubated with ethanol as the sole carbon source (*SI Appendix*, Fig. S5). Notably, ethanol provided most of the cytoplasmic and mitochondrial acetyl-CoA (23), and the presence of acetyl-CoA promoted *CLN3* transcription (24). Based on these observations, we hypothesize that the acceleration of ethanol metabolism is driven by the requirement to produce more acetyl-CoA, which is a response of *CLN3* knockout feedback regulation. The enhanced supply of acetyl-CoA would be beneficial for synthesizing most lipophilic compounds. Indeed, there is a significant increase in the level of acetyl-CoA (71.8%) and the production of total carotenoids (41%) in the H01 strain compared to the Z021 strain (Fig. 2*E* and *SI Appendix*, Fig. S9). Taken together, these results collectively suggest the occurrence of a strategic redistribution of energy and nutrients, laying a promising foundation for the production of lipophilic compounds.

The Stability and Universality of Strategies for Prolonging G1 Phase to Improve the Production of Lipophilic Compounds. The cell cycle is intricately regulated, with the potential for cell cycle progression to be reinstated over successive generations (25). This aspect is particularly significant when evaluating a strain's reliability as a robust platform for generating high-value products. To rigorously assess this, we conducted a study in which H01 cells were passaged for 600 generations (Fig. 2*F*), closely monitoring the total protein content and carotenoid production. The results confirmed that strains with a prolonged G1 phase, achieved through *CLN3* deletion, exhibited marked and heritable stability across 600 generations (Fig. 2*G*).

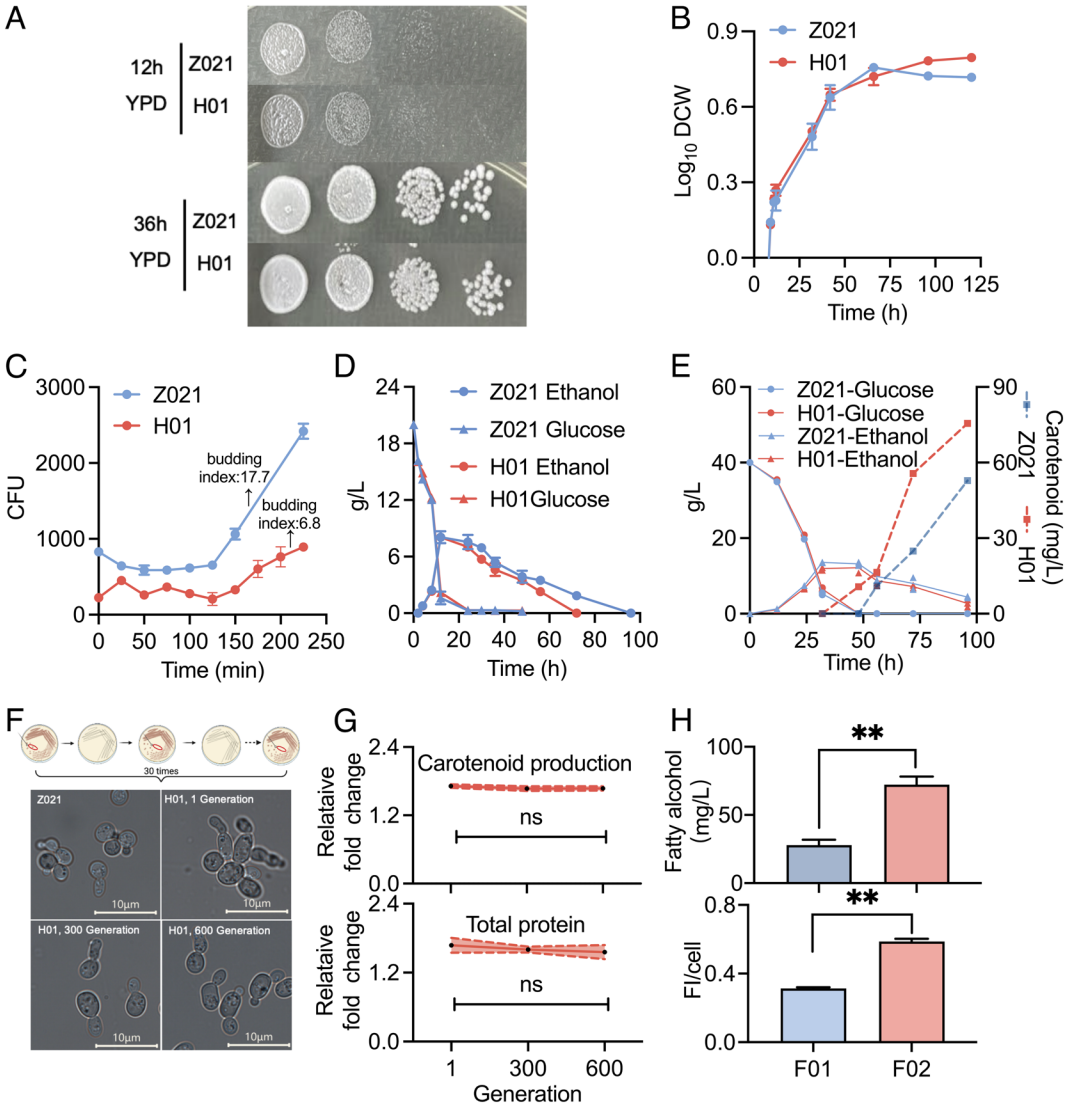

Fig. 2. Balancing cell division, growth and protein production facilitates the production of lipophilic compounds. (*A*) Sequential tenfold dilutions of Z021 and H01 were incubated on YPD plate at 30 °C. (*B*) Growth curves of the Z021 and H01 strains cultured in YPD medium. (*C*) Analysis of colony-forming units (CFUs) on YPD plates subsequent to varied periods of synchronized culture cycles for Z021 and H01, alongside determination of the budding index based on the gradient's slope (125 to 225 min). (*D*) Concentration curves of glucose and ethanol of the Z021 and H01 strains cultured in YPD medium. (*E*) Concentration curves of glucose and ethanol of the Z021 and H01 strains cultured in YPDG medium. The initiation of galactose-induced carotenoid production in YPDG medium exclusively occurs in the ethanol phase, which is attributed to the inhibition of the *GAL* promoter by the presence of glucose. YPDG: YPD supplemented with galactose. Z021, the control strain, harbors a carotenoid pathway controlled by the *GAL* promoter; H01, Z021 with the *CLN3* gene knocked out. Morphology (*F*), carotenoid production, and total protein content (*G*) of the H01 strain over 600 generations. Relative fold change: the change of H01 relative to Z021. (*H*) The effect of G1 extension for fatty alcohol production (*Upper*) and the expression of exogenous enzyme fatty acyl-CoA reductase (*Lower*). F01 and F02 were cultured in SC-Leu medium, and the production of fatty alcohol in these strains was measured at 96 h. The expression of fatty acyl-CoA reductase (FAR) was evaluated using fluorescence intensity (FI) of red fluorescence protein (RFP) by constructing the fusion protein FAR-RFP. The FI was measured at 48 h of culture. F01:CENPK2-1C harboring the pRS415-P_{pgk1}-*TaFAR*-linker-*RFP*-T_{gpd} plasmid; F02: F01, △*cln3*. *SI Appendix*, Table S1 presents the data from *E* and *H* in both the unit of per biomass and per cell. The data are representative of three independent experiments performed in triplicate. Statistical analysis was performed using a two-tailed Student's *t* test (**P* < 0.05, ***P* < 0.01, ****P* < 0.001, ns = no significance). The error bars represent the SD from the mean.

Furthermore, we explored the applicability of *CLN3* deletion for fatty alcohol production. The results demonstrated that, compared with the control strain, the deletion of *CLN3* (F02) resulted in a 159% increase in fatty alcohol production (Fig. 2*H* and *SI Appendix*, Fig. S6), and the expression of the exogenous enzyme fatty acyl-CoA reductase increased by 69% (Fig. 2*H*). These results collectively underscore the robustness and applicability of adopting *CLN3* deletion to induce G1 extension as a strategy to enhance lipophilic production in yeast cells.

Transcriptomic Analysis Revealed Cellular Reconfiguration for Adaptation to the Increased Protein Synthesis and Cell Volume. To gain deeper insights into the heightened protein synthesis and alterations in cell volume, we performed a transcriptomic analysis. Notably, deletion of the *CLN3* gene alone resulted in transcriptional changes affecting approximately half of the genome, with 1,569 genes upregulated and 1,514 genes downregulated. Specifically, the G1 cyclin-encoding gene *CLN1* was downregulated, while the repressor of G1 transcription-encoding gene *WHI5* was upregulated, which delayed the transition from the G1 phase to the S phase. Moreover, the chitin synthase-encoding gene *CHS1*, involved in the synthesis of the cell wall component chitin, and the *ERG3* and *ERG5* genes, involved in the synthesis of the cell membrane component ergosterol, were upregulated, which aligns with the observed increase in cell size. Kyoto Encyclopedia of Genes and Genomes (KEGG) enrichment analysis revealed that the differentially expressed genes (DEGs) were predominantly associated with genetic information processing and metabolism categories (Fig. 3*A*). Notably, the most

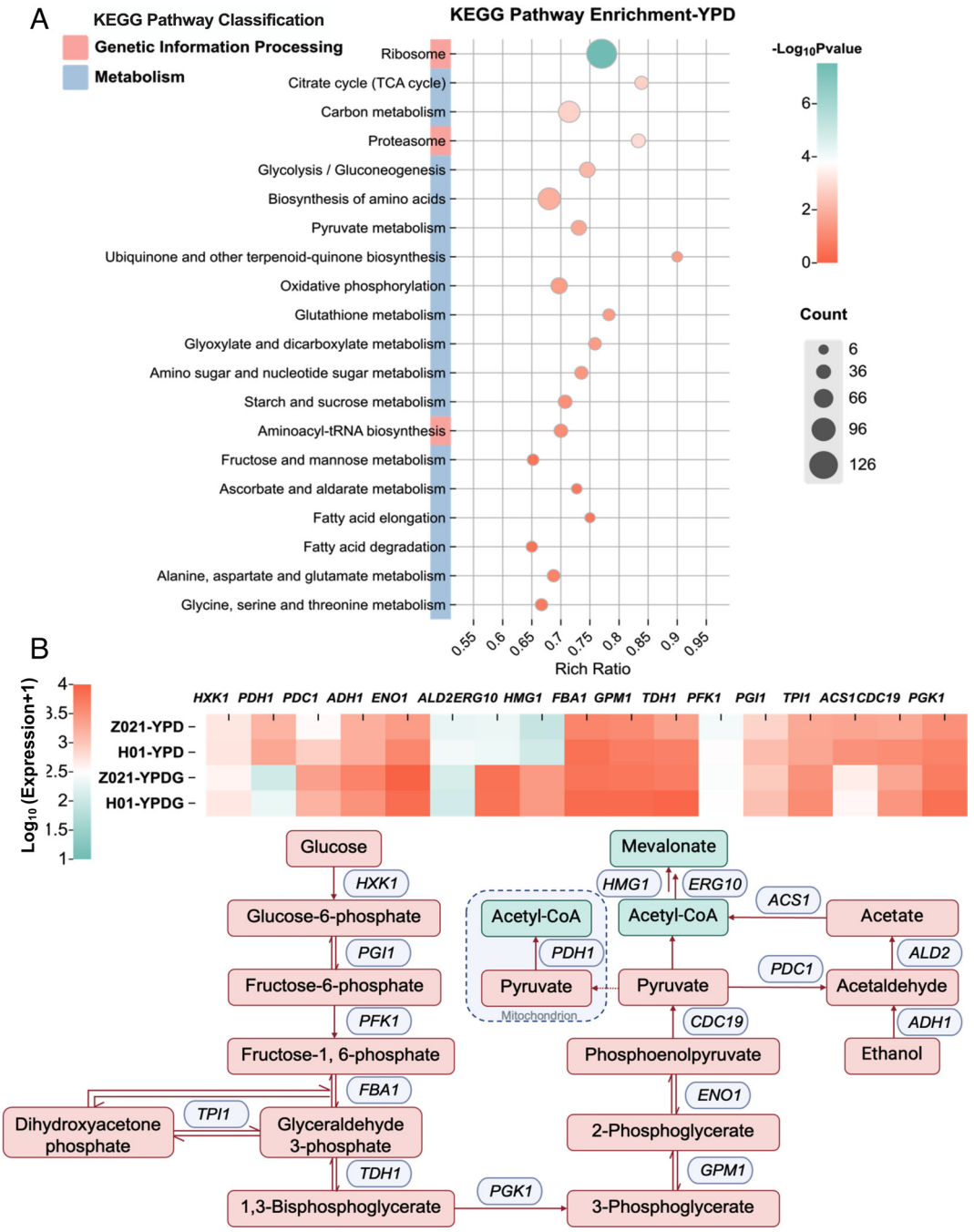

Fig. 3. Transcriptome analysis revealed cellular reconfiguration for adaptation to the increased protein synthesis and cell volume. (*A*) A KEGG enrichment analysis contrasting the H01 strain against the Z021 strain in YPD medium. The *X*-axis represents the enrichment ratio, and the *Y*-axis represents the specific KEGG pathway. The size of the bubble correlates with the number of genes annotated within each KEGG pathway, and the bubble color represents the statistical significance of the enrichment (*P* value). (*B*) Transcriptional alterations in genes involved in the formation of acetyl-CoA and mevalonate, shown with changes in gene expression (*Upper*) and metabolic pathway (*Lower*). For each strain (Z021 and H01), samples were collected from both YPD and YPDG cultures, at the stationary phase (48 h for YPD, 72 h for YPDG). Z021, the control strain, harbors a carotenoid biosynthetic pathway controlled by the *GAL* promoter; H01, Z021 with the *CLN3* gene disrupted. Z021-YPD: Z021 cultured in YPD medium; H01-YPD: H01 cultured in YPD medium; Z021-YPDG: Z021 cultured in YPDG (YPD supplemented with galactose) medium; H01-YPDG: H01 cultured in YPDG medium. "Expression" in the legend is the value of transcripts per million reads of the gene, and color intensity represents the gene expression level.

significant distinctions were observed in ribosomal components, including ribosome biogenesis and ribosomal subunits, highlighting the close link between ribosomes and protein synthesis during the prolonged G1 phase. Meanwhile, significant changes were also found in the expression levels of genes governing crucial processes such as transcription, translation, protein folding, sorting, and degradation (*SI Appendix*, Fig. S7).

Upon activation of exogenous carotenoid pathways in YPDG medium, which occurs due to galactose-induced transcription via the *GAL* promoter, transcriptional profiling revealed a consistent trend, with distinct variations in the genetic information processing category. Notably, in the YPD group, alterations were discernible in translation, while the YPDG group exhibited differences in protein folding, sorting, and degradation (*SI Appendix*, Fig. S8). Interestingly, genes involved in protein folding and quality control, such as *KAR2, PDI1,* and *ERO1*, were downregulated in the YPD group but upregulated in the YPDG group. Based on these observations, we hypothesize that the expression of heterologous

proteins might have imposed an additional burden on the cells. Previous studies have implicated that augmented cell dimensions correlate with a concerted enhancement in RNA and protein biosynthesis (8), further supporting our hypothesis.

Based on the transcriptional profiling, it can be inferred that the increase in total protein content subsequent to the extension of the G1 phase is potentially attributable to alterations in the expression of genes responsible for translation, protein folding, sorting, and degradation. Additionally, cell size emerges as a pivotal factor influencing metabolic adaptations (26), reinforced by the involvement of 2,129 DEGs in various metabolic processes. Notably, we observed a pronounced upregulation of glycolysis and a downregulation of the tricarboxylic acid cycle. Among the most remarkable findings was the significant upregulation of acetyl-CoA production pathways, including via pyruvate, acetic acid, and ethanol metabolism (Fig. 3*B*). To be specific, key genes such as *PDH1* for pyruvate dehydrogenase, *PDC1* for pyruvate decarboxylase, and *ADH1*, *ALD2*, and *ACS1* involved in ethanol metabolism exhibited upregulation. Quantitatively, on a per cell basis, the level of acetyl-CoA in the H01 strain was 71.8% higher compared to the Z021 strain (*SI Appendix*, Fig. S9). Moreover, a substantial upregulation of *HMG1* and *ERG10* was observed, indicating a robust enhancement in the expression of genes associated with the mevalonate (MVA) metabolic pathway. We hypothesize that the heightened demand for ergosterol may have promoted the upregulation of both acetyl-CoA and MVA synthesis pathways. In summary, our findings elucidated how ribosome biogenesis and enhanced ribosomal activity contribute to increased protein expression at the transcriptional level. Parallelly, the redirection of carbon metabolic flow toward the MVA pathway underscores the potential of G1 extension to facilitate the production of compounds that exploit the MVA pathway.

The Extended G1 Phase Improved Recombinant Synthesis through the Activated UPR. Transcriptomic analysis revealed that there is a upregulation of genes associated with protein folding and protein biosynthesis in the strain H01, suggesting the potential for the application of H01 for the expression of heterologous pathway enzymes. Thus, we tested the expression of exogenous enzymes in the Z02 and H01 strains by constructing the fusion protein, CrtE-red fluorescence protein (RFP), CrtY-RFP, CrtB-RFP, CrtI-RFP, and CrtZ-RFP (resulting in the Z1 to Z5 and H1 to H5 strain. Fig. 4*A* and *SI Appendix*, Fig. S10). Meanwhile, to avoid the interfere from the strength change of *GAL* promoter, we also introduced RFP controlled by the *GAL* promoter in the Z021 and H01 strains (resulting in the Z6 and H6 strain). Notably, between the background strain Z021 and H01, we observed slight alteration in the *GAL* promoter strength (Fig. 4*B*), but did observe significant increases in the expression levels of all the exogenous enzymes (Fig. 4*A*). Moreover, both the transcriptome and qPCR results showed that the UPR regulatory gene *HAC1* (27) was significantly upregulated (*SI Appendix*, Fig. S11). UPR is crucial for improving heterologous protein expression (Fig. 4*C*) and involves genetic regulation related to ER-associated degradation (ERAD), ER chaperones, and lipid synthesis (28). In consistent with this, our results also demonstrated the upregulation of genes associated with ER chaperones and ERAD (such as *YDJ1*, *KAR2*, and *ERO1*; *SI Appendix*, Table S2), together with lower ER content and higher lipid droplet (LD) content in H01 compared to Z021(Fig. 4 *D* and *E*).

Previous studies (29) have demonstrated that the ER serves as a crucial site for heterologous protein expression and lipophilic compound production. We thus attempted to enhance ER size to facilitate carotenoid production. We first regulated the expression levels of the UPR targets *INO2* and *OPI1* (30) to expand the ER. However, this intervention adversely affected cell growth (*SI Appendix*, Fig. S12) and significantly decreased carotenoid production (Fig. 4*F*). Then, it was found that the overexpression of *INO1* led to ER expansion, alongside a significantly decreased carotenoid production. In parallel, the genetic modification of genes responsible for the synthesis of phosphatidic acids (*ICE2* and *PAH1*) (31), precursors for phospholipid and acylglycerol lipids, achieved ER expansion, and did not impact cell growth or carotenoid production (Fig. 4*F* and *SI Appendix*, Fig. S12). These modifications above showed varied impacts in the LD content (Fig. 4*E*). These results indicate that the key factor influencing carotenoid production was the improved expression of pathway enzymes rather than lipid homeostasis. Subsequently, we overexpressed ER chaperones and genes involved in ERAD and UPR pathways, such as *YDJ1* (32) and *PDI1* (33), to improve recombinant protein expression, which led to a further augmentation in carotenoid production (Fig. 4*F*). This finding supports the hypothesis that the enhanced protein folding ability constituted the primary mechanism for enhanced carotenoid production, which is in consistent with the transcriptome and qPCR results in the *Δcln3* strain.

Discussion

In this study, we investigated how extending the G1 phase enhances the production of lipophilic compounds by enabling cells to adapt through resource allocation, metabolic recombination, and UPR activation. Specifically, deletion of the G1 cyclin *CLN3* effectively prolonged the G1 phase, resulting in higher cell size, DCW, and recombinant protein expression.

One notable observation following *CLN3* deletion was the upregulation of acetyl-CoA synthesis. It has been reported that acetyl-CoA-derived metabolites play a crucial role in stimulating the transcription of *CLN3*, ribosomal genes, and other growth-related genes through histone acetylation (24). Thus, the upregulation of acetyl-CoA synthesis observed in our study may suggest potential feedback regulation triggered by *CLN3* deletion. Furthermore, we reported an upregulation of the UPR following *CLN3* deletion. Previous studies have shown that protein synthesis occurs predominantly in the G1 phase of the cell cycle (34). The prolonged G1 phase caused by *CLN3* deletion in this study likely extended the process of protein synthesis for both endogenous and recombinant heterologous proteins, triggering the UPR to maintain physiological equilibrium. Interestingly, we noticed an increase in the abundance of LDs in yeast cells (Fig. 4*E*). Previous studies have demonstrated that LDs can sequester unfolded proteins and facilitate their degradation via microlipophagy (μLP) (35). Our transcriptome data also revealed the upregulation of *VPS4*, a gene associated with μLP (36), suggesting a potential mechanism for restoring protein homeostasis through LD-mediated protein degradation. We speculate that this response may also involve a balanced regulation of lipid metabolism to meet the higher demands for membrane integrity and function in larger cells.

This study evaluated the impact of *CLN3* deletion in shake flask cultures. However, the conditions of industrial production differ from those of shake flask culture. For example, while our study used a complex medium and ample glucose, industrial applications typically involve sugar-limited fed-batch cultures. During the cell culture, glucose is the primary carbon and energy source for yeast cells, and its concentration affects the cell growth rate. Inadequate glucose levels may lead to insufficient amino acid supply, impacting protein synthesis (37). Therefore, *CLN3* knockout strains under sugar-restricted conditions need to be tested for further

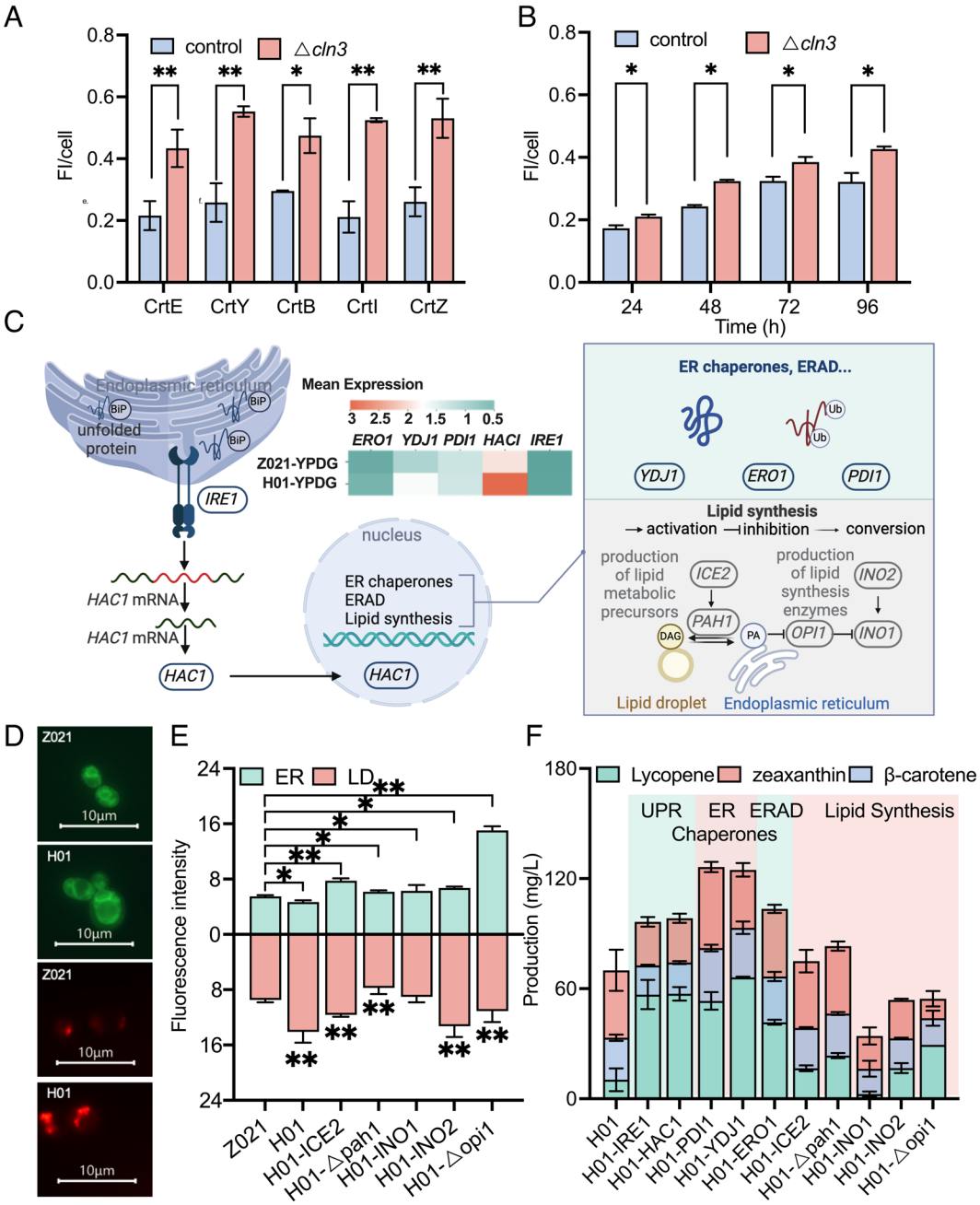

Fig. 4. The extended G1 phase improved recombinant protein synthesis through the activated UPR. (*A*) Determination of the enzyme expression level. The expression level was evaluated using the FI of RFP by constructing the corresponding fusion protein. After 72 h of incubation, the FI was measured in the strain Z1–Z5 and H1–H5. The control strains Z1, Z2, Z3, Z4, and Z5 harbor the fusion enzymes of the carotenoid pathway (CrtE-RFP, CrtY-RFP, CrtB-RFP, CrtI-RFP, and CrtZ-RFP), respectively, all controlled by the *GAL* promoter. H1, H2, H3, H4, and H5 were obtained by knockout of *CLN3* gene in Z1, Z2, Z3, Z4, and Z5. (*B*) Determination of the *GAL1* promoter strength. The expression level was evaluated using FI of RFP, using a GFP construct controlled by the *GAL1* promoter. After various incubation times, FI was measured in the Z6 and H6 strains. The control strain Z6 harbors a carotenoid pathway and an RFP expression cassette, both controlled by the *GAL* promoter. H6 was obtained by knockout of *CLN3* gene in Z6. (*C*) Schematic representation of ER stress in *CLN3* gene knockout cells expressing heterologous protein. (*D*) Fluorescence microscopy images of liposomes and the ER in H01 and Z021 after 48 h of incubation. The ER was stained with DiOC6, and the liposomes were stained with Nile red. (*E*) FI measurements after staining the ER and liposome contents of the strains. Strains shown underwent genetic modifications for UPR and biosynthesis of phosphatidic acids in H01 and were collected after 48 h of incubation. (*F*) Carotenoid production in H01-derived strains cultured in YPDG medium for 96 h. Strains shown underwent genetic modifications for UPR, ER stress, ERAD and lipid synthesis in H01. Z021, the control strain, harbors a carotenoid pathway controlled by the *GAL* promoter; H01, Z021 with the *CLN3* gene disrupted; The data are representative of three independent experiments performed in triplicate. Statistical analysis was performed using a two-tailed Student's *t* test (*$P < 0.05$, **$P < 0.01$, ***$P < 0.001$). The error bars represent the SD from the mean.

exploration. In addition, the oxygen concentration affects the redox state within the cell, which affects protein folding (38). Industrial oxygen conditions vary from those used in shake flask cultures, necessitating testing the performance of *CLN3* knockout strains under different oxygen concentrations in the future.

Overall, our study demonstrates that the extension of the G1 phase through *CLN3* deletion improves protein synthesis, lipid biosynthesis, and cell size, thereby significantly enhancing the ability of yeast to synthesize lipophilic compounds. This study may also serve as a valuable reference for investigating other eukaryotes, such as *Yarrowia lipolytica*. *Y. lipolytica,* known for its lipid uptake and utilization capabilities (39), has a higher lipid content compared to *S. cerevisiae* (40). Targeting genes with similar functions to *CLN3* in *Y. lipolytica* could potentially enhance the

production of lipophilic compounds in this yeast. Furthermore, in addition to the deletion of *CLN3*, other targeted genetic modification or metabolic engineering strategies could be explored to fine-tune the duration of specific cell cycle phases, thereby maximizing biomanufacturing capabilities while minimizing cell stress. Alongside this process, integrated systems biology approaches, including transcriptomic, proteomic, and metabolomic analyses, can provide a comprehensive understanding of the complex regulatory networks that control cell physiology and metabolite biosynthesis. Exploring the potential applications of our findings in different microbial systems and industrial settings through interdisciplinary approaches and innovative technologies could pave the way for the development of promising biotechnological solutions for efficient and sustainable bioproduction.

Materials and Methods

A detailed *Materials and Methods* section is provided in *SI Appendix*. Briefly, for the DNA manipulation of yeast strains in the study, genome integration and knockout were performed using CRISPR-Cas9. To determine product yield, carotenoid-producing strains were cultured in YPD medium supplemented with galactose (YPDG). Carotenoid analysis was carried out via high-performance liquid chromatography (HPLC). The concentrations of residual glucose, ethanol, acetate, and glycerol in the medium were analyzed via HPLC. Fatty alcohol-producing strains were cultured in synthetic complete medium lacking L-leucine (SC-Leu medium) supplemented with 10% dodecane. The organic phase was diluted 10-fold with n-hexane, and assessed via Gas Chromatography–Mass Spectrometry. The samples were sent to BGI Corporation (Wuhan, China) for transcriptomic analysis.

Data, Materials, and Software Availability. All study data are included in the article and/or *SI Appendix*. The detailed transcriptome is available at https://www.ncbi.nlm.nih.gov/bioproject/PRJNA1178133 (41).

ACKNOWLEDGMENTS. This work was supported by the National Key Research and Development Program of China (2021YFC2101000), the National Natural Science Foundation of China (22178261 & 22261142667), and the Key-Area Research and Development Program of Guangdong Province (2020B0303070002). We thank Jiazhang Lian for critical discussion. Graphics in Figs. 1*A* and 4*C* were created using BioRender software (BioRender.com).

Author affiliations: [a]Frontier Science Center for Synthetic Biology and Key Laboratory of Systems Bioengineering (Ministry of Education), School of Chemical Engineering and Technology, Tianjin University, Tianjin 300072, China; [b]Frontier Research Institute for Synthetic Biology, Tianjin University, Tianjin 300072, China; [c]College of Life Science and Technology, Beijing Advanced Innovation Center for Soft Matter Science and Engineering, Beijing University of Chemical Technology, Beijing 100029, China; [d]Department of Life Sciences, Chalmers University of Technology, Gothenburg SE41296, Sweden; [e]BioInnovation Institute, Copenhagen DK2200, Denmark; [f]School of Life Sciences, Faculty of Medicine, Tianjin University, Tianjin 300072, China; and [g]Georgia Tech Shenzhen Institute, Tianjin University, Shenzhen 518071, China

1. U. Münzner, E. Klipp, M. Krantz, A comprehensive, mechanistically detailed, and executable model of the cell division cycle in *Saccharomyces cerevisiae*. *Nat. Commun.* **10**, 1308 (2019).
2. J. Kalucka *et al.*, Metabolic control of the cell cycle. *Cell Cycle* **14**, 3379–3388 (2015).
3. A. Litsios *et al.*, Differential scaling between G1 protein production and cell size dynamics promotes commitment to the cell division cycle in budding yeast. *Nat. Cell Biol.* **21**, 1382–1392 (2019).
4. J. O. Patterson, S. Basu, P. Rees, P. Nurse, CDK control pathways integrate cell size and ploidy information to control cell division. *Elife* **10**, e64592 (2021).
5. X. Liu *et al.*, Reliable cell cycle commitment in budding yeast is ensured by signal integration. *Elife* **4**, e03977 (2015).
6. M. Kõivomägi, M. P. Swaffer, J. J. Turner, G. Marinov, J. M. Skotheim, G1 cyclin–Cdk promotes cell cycle entry through localized phosphorylation of RNA polymerase II. *Science* **374**, 347–351 (2021).
7. K. M. Schmoller, J. J. Turner, M. Kõivomägi, J. M. Skotheim, Dilution of the cell cycle inhibitor Whi5 controls budding-yeast cell size. *Nature* **526**, 268–272 (2015).
8. G. E. Neurohr *et al.*, Excessive cell growth causes cytoplasm dilution and contributes to senescence. *Cell* **176**, 1083–1097.e18 (2019).
9. Y. Shi *et al.*, Production of plant sesquiterpene lactone parthenolide in the yeast cell factory. *ACS Synth. Biol.* **11**, 2473–2483 (2022).
10. J. Hong, S.-H. Park, S. Kim, S.-W. Kim, J.-S. Hahn, Efficient production of lycopene in *Saccharomyces cerevisiae* by enzyme engineering and increasing membrane flexibility and NAPDH production. *Appl. Microbiol. Biotechnol.* **103**, 211–223 (2019).
11. M. Li, P. Zhou, M. Chen, H. Yu, L. Ye, Spatiotemporal regulation of astaxanthin synthesis in *S. cerevisiae*. *ACS Synth. Biol.* **11**, 2636–2649 (2022).
12. A. Read, M. Schröder, The unfolded protein response: An overview. *Biology* **10**, 384 (2021).
13. T. Yu *et al.*, Metabolic reconfiguration enables synthetic reductive metabolism in yeast. *Nat. Metab.* **4**, 1551–1559 (2022).
14. N. Slavov, D. Botstein, Coupling among growth rate response, metabolic cycle, and cell division cycle in yeast. *Mol. Biol. Cell* **22**, 1997–2009 (2011).
15. L. Cai, B. P. Tu, Driving the cell cycle through metabolism. *Annu. Rev. Cell Dev. Biol.* **28**, 59–87 (2012).
16. F. Bezold *et al.*, Optogenetic control of Cdc48 for dynamic metabolic engineering in yeast. *Metab. Eng.* **79**, 97–107 (2023).
17. Y. Sun *et al.*, Enhanced production of β-carotene in recombinant *Saccharomyces cerevisiae* by inverse metabolic engineering with supplementation of unsaturated fatty acids. *Process Biochem.* **51**, 568–577 (2016).
18. M. Kafri, E. Metzl-Raz, G. Jona, N. Barkai, The cost of protein production. *Cell Rep.* **14**, 22–31 (2016).
19. G. Liti *et al.*, Population genomics of domestic and wild yeasts. *Nature* **458**, 337–341 (2009).
20. A. I. Goranov *et al.*, The rate of cell growth is governed by cell cycle stage. *Genes Dev.* **23**, 1408–1422 (2009).
21. M. Kavšček, M. Stražar, T. Curk, K. Natter, U. Petrovič, Yeast as a cell factory: Current state and perspectives. *Microb. Cell Fact.* **14**, 94 (2015).
22. S. Klumpp, M. Scott, S. Pedersen, T. Hwa, Molecular crowding limits translation and cell growth. *Proc. Natl. Acad. Sci. U.S.A.* **110**, 16754–16759 (2013).
23. T. Xiao, A. Khan, Y. Shen, L. Chen, J. D. Rabinowitz, Glucose feeds the tricarboxylic acid cycle via excreted ethanol in fermenting yeast. *Nat. Chem. Biol.* **18**, 1380–1387 (2022).
24. L. Shi, B. P. Tu, Acetyl-CoA induces transcription of the key G1 cyclin CLN3 to promote entry into the cell division cycle in *Saccharomyces cerevisiae*. *Proc. Natl. Acad. Sci. U.S.A.* **110**, 7318–7323 (2013).
25. C. Garmendia-Torres, O. Tassy, A. Matifas, N. Molina, G. Charvin, Multiple inputs ensure yeast cell size homeostasis during cell cycle progression. *Elife* **4**, e34025 (2018).
26. M. J. Brauer *et al.*, Coordination of growth rate, cell cycle, stress response, and metabolic activity in yeast. *Mol. Biol. Cell.* **19**, 352–367 (2008).
27. L. Matabishi-Bibi, D. Challal, M. Barucco, D. Libri, A. Babour, Termination of the unfolded protein response is guided by ER stress-induced HAC1 mRNA nuclear retention. *Nat. Commun.* **13**, 6331 (2022).
28. H. Wu, B. S. H. Ng, G. Thibault, Endoplasmic reticulum stress response in yeast and humans. *Biosci. Rep.* **34**, e00118 (2014).
29. H. Wang *et al.*, Systematic engineering to enhance 8-hydroxygeraniol production in yeast. *J. Agric. Food Chem.* **71**, 4319–4327 (2023).
30. S. Schuck, W. A. Prinz, K. S. Thorn, C. Voss, P. Walter, Membrane expansion alleviates endoplasmic reticulum stress independently of the unfolded protein response. *J. Cell Biol.* **187**, 525–536 (2009).
31. D. Papagiannidis *et al.*, Ice2 promotes ER membrane biogenesis in yeast by inhibiting the conserved lipin phosphatase complex. *EMBO J.* **40**, e107958 (2021).
32. D. Gaur *et al.*, The yeast Hsp70 cochaperone Ydj1 regulates functional distinction of Ssa Hsp70s in the Hsp90 chaperoning pathway. *Genetics* **215**, 683–698 (2020).
33. Y. Lin, Y. Feng, L. Zheng, M. Zhao, M. Huang, Improved protein production in yeast using cell engineering with genes related to a key factor in the unfolded protein response. *Metab. Eng.* **77**, 152–161 (2023).
34. K. Campbell *et al.*, Building blocks are synthesized on demand during the yeast cell cycle. *Proc. Natl. Acad. Sci. U.S.A.* **117**, 7575–7583 (2020).
35. E. J. Garcia *et al.*, Membrane dynamics and protein targets of lipid droplet microautophagy during ER stress-induced proteostasis in the budding yeast, *Saccharomyces cerevisiae*. *Autophagy* **17**, 2363–2383 (2021).
36. J. D. Vevea *et al.*, Role for lipid droplet biogenesis and microlipophagy in adaptation to lipid imbalance in yeast. *Dev. Cell* **35**, 584–599 (2015).
37. I. Yoon *et al.*, Glucose-dependent control of leucine metabolism by leucyl-tRNA synthetase. *Science* **367**, 205–210 (2020).
38. C. Picazo, M. Molin, Impact of hydrogen peroxide on protein synthesis in yeast. *Antioxidants* **10**, 952 (2021).
39. A. M. Worland *et al.*, Analysis of *Yarrowia lipolytica* growth, catabolism, and terpenoid biosynthesis during utilization of lipid-derived feedstock. *Metab. Eng. Commun.* **11**, e00130 (2020).
40. A. Fabiszewska, P. Misiukiewicz-Stępień, M. Paplińska-Goryca, B. Zieniuk, E. Białecka-Florjańczyk, An insight into storage lipid synthesis by *Yarrowia lipolytica* yeast relating to lipid and sugar substrates metabolism. *Biomolecules* **9**, 685 (2019).
41. H. Hao, Data from "Extending the G1 phase improves the production of lipophilic compounds in yeast by boosting enzyme expression and increasing cell size." NCBI. https://www.ncbi.nlm.nih.gov/bioproject/PRJNA1178133. Deposited 26 October 2024.